Identification and analysis of ghost reflection in the interferometers based on ZEMAX by optimization algorithms

Enming Zhang,[a,b] Weinan Ye,[a,b] Yizhou Xia,[a,b] Leijie Wang,[a,b] and Ming Zhang[a,b,*]

[a]Tsinghua University, State Key Laboratory of Tribology in Advanced Equipment, Beijing, China

[b]Tsinghua University, Beijing Lab of Precision/Ultra-Precision Manufacture Equipment and Control, Beijing, China

Abstract. Laser interferometers and grating interferometers based on optical interferometry are widely used in displacement measurement of precision machining and testing equipment, such as the measurement system of integrated circuit equipment, due to their high precision, noncontact, and large dynamic measurement range. The ghost reflection in optical elements may lead to the periodic nonlinear error of the interferometer and also reduce alternating current/direct current. We propose a general method for automatic ghost reflection interface identification. It can analyze the influence weight of ghost reflection for each interface of any interferometer. In addition, the manufacturing cost of the interferometer is effectively reduced by optimization algorithms that enable ghost reflection avoidance in the interferometer design. Experimental results prove the influence weight of ghost reflection at different positions in the interferometer and provide the parameter selection of the most suitable interface reflection of the interferometer.
© *The Authors. Published by SPIE under a Creative Commons Attribution 4.0 International License. Distribution or reproduction of this work in whole or in part requires full attribution of the original publication, including its DOI.* [DOI: 10.1117/1.OE.62.3.034103]

Keywords: interferometer; ghost reflection; algorithm optimization; measurement error; ZEMAX.

Paper 20221418G received Dec. 7, 2022; accepted for publication Feb. 6, 2023; published online Mar. 6, 2023.

1 Introduction

Optical interferometry technology is widely used in displacement measurement, such as microelectromechanical systems, atomic force microscopy, gravitational wave detection, and integrated circuit equipment. It shows the advantages of high precision, noncontact, and large dynamic measurement range. The interferometer is one of the most commonly used precision instruments for ultraprecise displacement measurement. Using different interference signal processing models, the interferometer can be categorized as either homodyne or heterodyne interferometer; according to the reflection of optical components that use mirrors or diffraction grating, it may also be divided into laser interferometer or grating interferometer.[1–5]

The principle of the interferometer is that the Doppler effect produced by the displacement of the object to be measured is brought into the interference signal through the interfering beams, which go through a specific structure lens group. The phase shift of the interference signal can be obtained through a certain phase demodulation calculation, and the measurement results of the object displacement can be calculated based on the displacement calculation model.[6,7] However, the nonideal factors in this process will affect the quality and accuracy of the measured signal of the interferometer.[8,9] The error phase shift leads to the superposition of Doppler frequency shift and error phase, so the calculated phase cannot accurately reflect the displacement of the object.[10] As an inevitable stray beam, ghost reflection affects alternating current (AC)/direct

*Address all correspondence to Ming Zhang, zhangm@tsinghua.edu.cn

current (DC) and produces measurement error, so suppressing the ghost reflection of the interferometer is of great significance.

The ghost reflection is related to the refractive index of adjacent media. The interface reflectance of common optical elements in interferometer ranges from 0.5% to 5%, which can be reduced to lower than 0.25% by coating in specific materials and wavelength ranges.[11] Researchers found that an optical system with 340 interfaces produces about 57,000 first-order ghosts.[12] The trend of multi-axis, integration, and high optical subdivision to achieve higher resolution causes the structure of the interferometer to become increasingly complex, and the number of interfaces increase rapidly.[13,14] When the number of interfaces in the interferometer increases, the number of ghost reflection light generated at each interface increases sharply.[12] In the imaging system, the optical path passes through the designed optical element in turn according to the sequence, and the analysis is relatively simple. In the interferometer, the laser may split and backtrack many times through the same optical element, such as a polarization beam splitter. In addition, the ghost of the imaging system is stray light that focuses outside the target signal; however, the ghost reflection in the interferometer will be directly superimposed on the target optical path, which makes it more difficult to analyze. In the field of imaging system, there are a large number of studies focus on the stray beam generated by a ghost reflection.[15–17] Few studies have systematically examined the influence weight of ghost reflection on interferometers.[15,18] Shapiro and Boyd[15] studied the ghost reflection process based on physics and found that some ghost reflection beams pass through the optical element and enter the detector with the measured interference beam, such that the received intensity of interference beams can be regarded as the superposition of the main beam and the stray ghost reflection beam. Hu et al.[18] studied the second-order Doppler frequency shift of a specific mirror and the corner cube retroreflector (CCR) model and found that the second-order frequency shift is caused by the second-order ghost reflection, while the second-order frequency shift of the mirror is generated by the first-order ghost reflection, and when the reflectivity of quarter wave plate (QWP) is set to 0.15%, the nonlinear error caused by ghost reflection in this structure is in nanoscale. Ghosting can also cause signal overlap, thus affecting the AC/DC of the interference signal, introducing high electronic noise in the measurement results, and even causes interferometer failure.[19] Thus, ghost reflection is of great significance in interferometer design. At present, the analysis of ghost reflection is almost dependent on automation methods, which relies heavily on the ability of designers; therefore, it is easy to miss some interfaces for complex systems. In addition, there is little previous research on ghost reflection error analysis of interferometers with a general structure, and thus few applicable methods to refer to. Therefore, a general and automatic ghost reflection analysis method is needed.

In interferometer measurement system, it is very important to research and develop a general method to automatically identify the position and energy of stray light generated by ghost reflection, to realize the quantitative analysis of the periodic nonlinear error of the measurement signal by ghost reflection. Thus, developing an optimization algorithm to improve design efficiency of ghost reflection is an effective method.[20]

In this paper, a general automatic method of identification is proposed that can be used in any interferometer to identify the ghost reflection and further analyze the effect of different reflections on the accuracy of the measurement. Finally, according to the analysis results, the manufacturing requirements of ghost reflection interface are given considering the measurement accuracy and manufacturing cost, and the balance between performance and cost is achieved. The effect of ghost reflection on interferometer signal and measurement resolution is analyzed. To reduce the operation complexity of the proposed method, a program is applied, which contains a convenient human–computer interaction and it greatly improves the analysis efficiency of ghost reflection in interferometer design. The experimental results show that the proposed method accurately reflects the influence weight of ghost reflection on an interferometer case and shows the method to be efficient. As a result, on the premise of ensuring the performance is basically unchanged, the manufacturing cost is reduced by 45%. Our optimizations can be applied to most interferometer structures. The researchers need to establish a model in the ZEMAX ray tracing software. After interacting with the model in ZEMAX and the MATLAB program, by changing component numbers and object interface numbers in order and technical specifications according to the needs, the location identification of ghosts and the weight

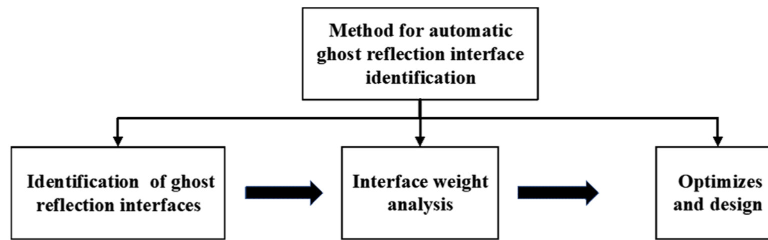

Fig. 1 Steps of the method for automatic ghost reflection interface identification.

analysis of measurement values can be realized. In addition, when they need to carry out the actual manufacturing cost control in optimization, the algorithm can achieve the lowest cost optimization under specific technical specifications.

2 Principle

2.1 *Analysis and Optimization Method of Ghost Reflection*

As shown in Fig. 1, the method has three steps. First, the interferometer interfaces have enumerated that laser through in the component for the identification to avoid missing the interface. Second, the interface weight analysis is carried out by specifying the reflectivity of every interface in turn and calculating the influence. Finally, the optimized design is achieved according to the optimal cost as the goal.

2.1.1 *Identification method of ghost reflection interfaces*

Ghost reflection can be divided into the following three types in the interferometers. The first one is the light leakage due to ghost reflection, in which the detector does not acquire the stray beam caused by ghost reflection. It generates energy loss of the laser beam and reduces AC/DC, but does not import periodic nonlinear error. The second type of stray beam is caused by acquisition of the ghost reflection by the detector along with the reference beam. It does not follow the designed optical path, which will change the equivalent optical path. However, due to the highly integrated design, the periodic nonlinear error it causes can be ignored, and it only exists in a few specific types of interferometers. The last kind of stray beam caused by ghost reflection is the measurement beam passing through the object to be measured. When the beam does not contain displacement information or nonideal displacement information acquired by the detector, it will cause periodic nonlinear error, which affects the measurement accuracy.

Therefore, the identification of ghost reflection first needs to determine each interface. In the method, the model was established based on ZEMAX ray tracing software, and all the interfaces were first sorted according to the sequence of laser passing. Every interface of the optical element that the laser passes will be recorded and analyzed in order. Therefore, this method solves the problem that the key ghost reflection interface may be missed by manual analysis for complex structures and the interface position is displayed by serial number.

2.1.2 *Ghost reflection influence analysis*

The identification of ghost reflections mentioned above requires periodic nonlinear error and AC/DC comparisons to analyze the effects of ghost reflections at each interface to achieve the identification. By assigning different reflectivity to each interface, all interfaces are used in the interface reflectivity setting. The ideal case of zero reflectivity is used as the control group. By comparing the model with the set of ghost reflectivity and by comparing the performance of the interferometer under different reflectivity of the interface, the influence weight of the measurement is quantitatively analyzed. By comparing the performance under different reflectivity, the interface with severe ghost reflection is identified, and the interface position is displayed by serial number, thus providing guidance for designers. The method is general and suitable for

any type of interferometers. In this study, we only take the two most representative interferometers of homodyne and heterodyne as examples. For other types, we can modify the model according to the principle of interferometer. The analysis method for the periodic nonlinear error and AC/DC of the interferometer is as follows.

Because the two beams are produced by the same laser, the frequency, f, the amplitude, A, and the initial phases, θ_1, θ_2 are the same for both. The two beams are expressed as

$$E_1 = Ae^{i\{2\pi[f+f_d(t)]t+\theta_1\}},\quad E_2 = Ae^{i(2\pi ft+\theta_2)}. \tag{1}$$

Phase discrimination by four detectors is an available method applied to the homodyne interferometer. It is well known that the homodyne optical structure can split the incident beam into four parts to form four interference fringes, and the phase difference of each group of interference fringes is 90 deg.

For the heterodyne interferometer, when the frequencies of the two beams are adjusted by the acousto-optic modulator, the frequencies of the two beams are set as f_1 and f_2. The two beams are expressed as

$$E_1 = Ae^{i\{2\pi[f_1+f_d(t)]t+\theta_1\}},\quad E_2 = Ae^{i(2\pi f_2 t+\theta_2)}. \tag{2}$$

The stray light generated by the ghost reflection is partially leaked, and the ghost reflection beam entering the detector is expressed as

$$\begin{aligned} E_g &= E_{g0} + E_{g1} + E_{g2} + E_{g3} + \dots \\ &= A_{g0}e^{i\{2\pi f_1 t+\theta_1\}} + A_{g1}e^{i\{2\pi[f_1+f_d(t)]t+\theta_1\}} + A_{g2}e^{i\{2\pi[f_1+2f_d(t)]t+\theta_1\}} \\ &\quad + A_{g3}e^{i\{2\pi[f_1+3f_d(t)]t+\theta_1\}} + \dots, \end{aligned} \tag{3}$$

where E_{g0} represents the optical vector without Doppler effect, E_{g1}, E_{g2}, and E_{g3} represent the optical vector with first-, second-, and third-order Doppler effect. Only the Doppler effect lower than third-order is expressed in the model. A_{g0}, A_{g1}, A_{g2}, and A_{g3} represent the amplitude of the ghost reflection, and θ_1 represents the phase of the ghost reflection.

To the two interference signals used for measurement, after the superposition of the two beams, the synthesized intensity of the beam remains unchanged and the intensity is affected by the initial phase. The intensity is expressed as

$$I = (E_1 + E_2)\overline{(E_1 + E_2)} = A_1^2 + A_2^2 + 2A_1A_2\cos(\theta_1 + \theta_2). \tag{4}$$

When considering ghost reflection, it can be regarded as three-light interference

$$I = (E_1 + E_2 + E_g)\overline{(E_1 + E_2 + E_g)}. \tag{5}$$

The phase demodulation can be realized by the operation of difference comparison. Two orthogonal signals are obtained by subtracting two sets of signals with phase difference of 180 deg. The variation φ of the phase of S polarized and P polarized is expressed as the light intensity $I_1 - I_4$

$$\varphi = \Delta\theta_{\mathrm{P}} - \Delta\theta_{\mathrm{S}} = \arctan\left(\frac{I_4 - I_2}{I_1 - I_3}\right), \tag{6}$$

where $\Delta\theta_{\mathrm{S}}$ and $\Delta\theta_P$ represent the variation of the phase of S polarized and P polarized, respectively. The phase shift of the measured beam is obtained by the homodyne phase calculate method.

When considering ghost reflection, the nonideal interference signals are coupled into light intensity, producing error in the known phase discrimination method.

When the mirror fixed on the moving object moves along the Z direction, the phase information introduced in the measurement beam is obtained as

$$\varphi = 2\pi \int f_d(t)\mathrm{d}t. \tag{7}$$

In this interferometer model, the calculated displacements are expressed as

$$z(t)_m = \frac{\varphi}{2n\pi}\lambda = \frac{\varphi}{8\pi}\lambda. \tag{8}$$

After calculating the displacement by intensity, the measurement error is expressed as

$$\mathrm{Error} = z(t)_r - z(t)_m, \tag{9}$$

where $z(t)_r$ represents the actual set displacement of the motion table, $z(t)_m$ represents the calculated displacement, n represents the optical subdivision, in this model $n = 4$, λ represents the wavelength of the laser.

The AC/DC of the interference signals should be considered in the measurement of the interferometer. It directly affects the quality of the AC signal used for phase calculation. When it is not high enough, it will lead to high electronic noise and even failure of measurement. The rotation angle generated by the mirror moving leads to the spot separation, and the angle between the interfering beams and the AC/DC of the signal will be affected. The spot separation makes that the two beams have no interference occurred, and the angle between the beams will form interference fringes. The interference signal used for phase calculation is the integral of the intensity in the coupling area of the detector. The appearance of the interference fringes will lead to an increase in the direct flow of the interference signal and the decrease of the AC amount. The decrease in AC/DC will lead to an increase in measurement uncertainty, and the high DC component will also increase the requirements for photoelectric detectors and other devices. AC/DC of interference signal is expressed as

$$\frac{\mathrm{AC}}{\mathrm{DC}} = \frac{I_{\mathrm{AC}}}{I_{\mathrm{DC}}} = \frac{\max(I) - \min(I)}{\max(I) + \min(I)}. \tag{10}$$

In the analysis of interfacial reflections of ghosts, the optical elements in an interferometer can be considered as three types: splitting, refractive, and polarization control elements, and can generally be classified as objects with more than two interfaces and two interfaces. Figure 2 shows a schematic diagram of the ghost generated by laser through two types of optical elements,

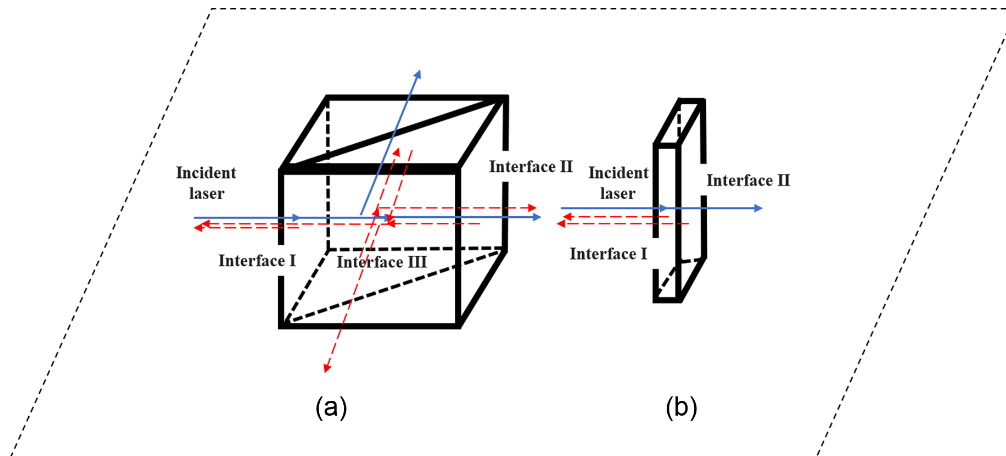

Fig. 2 Schematic diagram of optical path structure of laser through (a) more than two interface optical elements and (b) two interface optical elements.

in which the solid blue line represents the ideal light path and the dashed red line represents the ghost reflection.

2.1.3 *Optimization method*

Due to that the ghost reflection of each optical interface of the interferometer system will lead to the reduction of AC/DC and cause a periodic nonlinear error, thus affecting the measurement accuracy. Therefore, it is necessary to increase the transmittance of each interface as much as possible to suppress the nonideal optical path. Coating is a common way, but different antireflection film correspond to the manufacturing process and difficulty is directly related to the cost. With the premise of determining the technical specification of the interferometer, the upper limit of ghost reflectivity of each interface determines the cost of the interferometer. Because different interfaces in a complex interferometer have different weights for the measurement of the interferometer, it is necessary to develop an algorithm. Considered the production cost, the upper limit of ghost reflectivity of each optical interface that meets the technical specification of the interferometer is given. The influence of the interface of different optical elements on the measurement signal and the measurement accuracy is coupled, and as the number of optical elements increases, the influence of different interface reflectivity on the measurement results increases exponentially. For complex systems, to optimize the reflectivity of each interface efficiently, the genetic algorithm is used to optimize the ghost reflectivity of each interface of the known system. The single objective of the optimization is to minimize the manufacturing cost of each transmission interface of the system. The two constraints are that the measurement error is not higher than the required precision and the AC/DC value is not lower than the given technical specification. The two technical specifications are similar to some extent, but not positively correlated.

The investigation shows that the interface ghost reflectivity range of the optical element is 0% to 5%. We investigate commercial coating quotes from related optical companies, the relationship between reflectivity and manufacturing cost is nonlinear, which can be fitted by a piecewise function. The corresponding relationship between the reflectivity and manufacturing cost is expressed as

$$g(x) = \begin{cases} 1013.2x^2 - 2371x + 1913.6, & 0.1 < x \leq 1 \\ 77.86x^2 - 523.99x + 995.24, & 1 < x \leq 3 \\ 77.86x^2 - 523.99x + 995.24, & x \geq 3, \end{cases} \tag{11}$$

where x represents the reflectivity and the unit is %, $g(x)$ represents the manufacturing cost of the current interface reflectivity at an appropriate size and the unit is ¥.

Due to the limitation of manufacturing cost and manufacturing capacity, the technical specifications of most optical products with lens groups are limited by ghost reflectivity. By discretizing and parameterizing the decision variables, the optimization problem is transformed into a nonlinear programming problem. Because the actual reflectivity of each interface is discontinuous, 12 discrete points are taken in the interval of 0.1% to 5%; the above values are common coating specifications and can represent the actual situation better, which are defined as set D = [0, 0.001, 0.005, 0.01,0.015,0.02, 0.025, 0.03, 0.035, 0.04, 0.045, 0.05].

The decision variable X is expressed as

$$X = (x_1, x_2, \ldots, x_k)^T, \quad x_i \in D \tag{12}$$

The optimization objective $F(X)$ represents the manufacturing cost of the interferometer optical element at variable X, where k is the number of interfaces.

The objective min $F(X)$ of optimization and the constraints Error_X and AC/DC_X are expressed as

$$\min\, F(X) = \min\, F(x_1, x_2, \ldots, x_k) = g(x_1) + g(x_2) + \ldots g(x_k) = \min \sum_{i=1}^{k} g(x_i), \tag{13}$$

$$g(x) = -10.353x^5 + 143.29x^4 - 758.58x^3 + 1974.6x^2 - 2734.2x + 1941.1, \tag{14}$$

s.t.

$$\begin{cases} \text{Error}_X = f_\theta(X) = f_\theta(x_1, x_2, \dots, x_k) \le \text{Error}_{\max},\ x_i \in D \\ \text{AC/DC}_X = h_\theta(X) = h_\theta(x_1, x_2, \dots, x_k) \ge \text{AC/DC}_{\min},\ x_i \in D \\ x_i \in D,\ D = [0,\ 0.001,\ 0.005,\ 0.01, 0.015, 0.02,\ 0.025, 0.03,\ 0.035, 0.04, 0.045,\ 0.05]. \end{cases} \tag{15}$$

After constructing the optimization model, the genetic algorithm is initialized. Heuristic population initialization was adopted. The first generation generated the 12 populations above and 88 random populations with equal reflectivity to form an initial population of 100 groups X. Based on the amount of data and experience, we chose to set the number of the initial generation at 100 samples, of which we chose 12 samples that are set to the same known reflectivity as a subjective optimization behavior; to effectively determine the interferometer manufacturing range, the remaining 88 samples are selected to ensure that the genetic algorithm optimization comprehensive.

The objective function value $F(X)$ of the initial population is calculated. (The technical specification is calculated after ZEMAX ray tracing, and the objective function is calculated when the constraint condition is satisfied.) According to it, the fitness function of the initial population is set. (The optimal proportional selection method is adopted, and M individuals ($M \le 10$) with the minimum objective function $F(X)$ satisfying the constraint condition are selected.) The objective function values are arranged from large to small and assigned $1 - M$. The probability that the individual is selected can be expressed as

$$P_i = M_i / \sum_{j=1}^{M} M_i. \tag{16}$$

The retained individual was selected as the parent and the mother, and its chromosomes were extracted for crossover ($P_c = 0.6$) to produce offspring (exchange x_i). The chromosome of the offspring is mutated ($P_m = 0.6$), and the reservation with high fitness is screened. In the algorithm, subjective optimization is that when the known variable group does not satisfy the constraint condition, it no longer crosses and mutates in the direction of increasing variables, and when the objective function $F(X)$ of the known variable group and the known variable group is not higher than the existing variable group, it is no longer crossed and mutated in the direction of variable reduction (cost increase). And elite selection is used to retain the optimal individual in each iteration process.

Repeat the above steps until a new population is generated, and the termination condition is to complete the cycle after a given evolutionary generation or the optimal individual in the population is continuously not improved. The optimization process of interferometer manufacturing cost parameters based on the genetic algorithm is shown in Fig. 3.

2.2 *Implementation of Analysis and Optimization Method of Ghost Reflection*

The implementation of the method above requires a model based on ZEMAX ray tracing software. Therefore, a model is used for verification, which is established based on the cosimulation of ZEMAX ray tracing software in a nonsequential mode and MATLAB to verify the technical specification of the laser interferometer, including displacement measurement accuracy and angular tolerance performance.

2.2.1 *Automatic ghost reflection interface identification*

As shown in Fig. 4, the optical path structure of a typical interferometer is a quadruple optical subdivision interferometer based on the parallel reflection characteristics of the CCR.[4] The measured optical path passes through the object to be measured twice, and the upper and lower layers of the optical path are realized after passing through the CCR. The structure is compact,

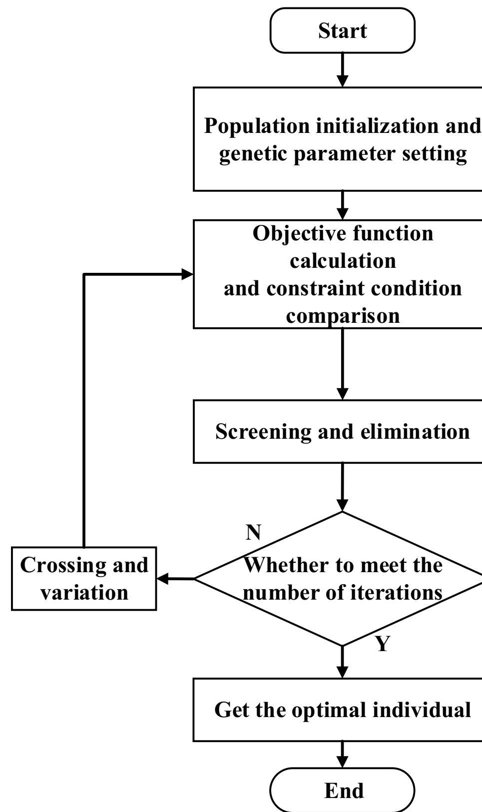

Fig. 3 Optimization process of influencing factor parameters based on genetic algorithm.

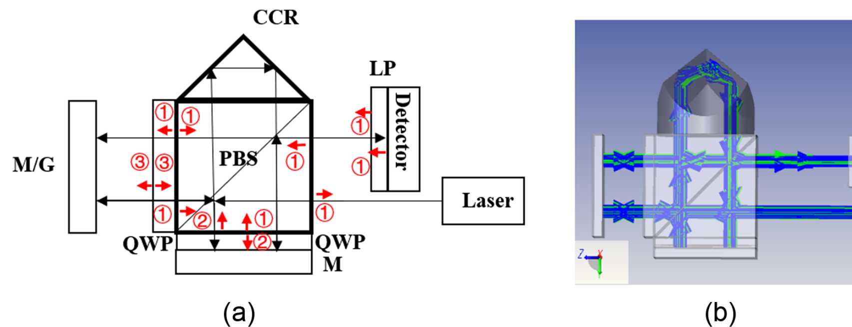

Fig. 4 (a) Schematic diagram of optical path structure of quadruple optical subdivision laser interferometer system. QWP, quarter wave plate; PBS, polarizing beam splitter; CCR, corner cube retroreflector; M, mirror; LP, linear polarizer. (b) Simulation optical configuration model with ZEMAX.

but it puts forward higher requirements for tooling and alignment. The geometric analysis of the optical path is carried out, including (1) representing the first ghost, (2) representing the second ghost, and (3) representing the third ghost.

The simulation model of the laser interferometer is shown in Fig. 4. The wavelength of the laser in the model is set to 780 nm, the diameter of the laser beam diameter is 1 mm, and the initial energy is 1 J. The frequency of the incident beam is expressed by f as the diameter of the photodetector is 1 mm. The mirror for measuring beam can move along the Z direction and rotate along the X, Y, and Z directions at a suitable speed under the control of MATLAB.

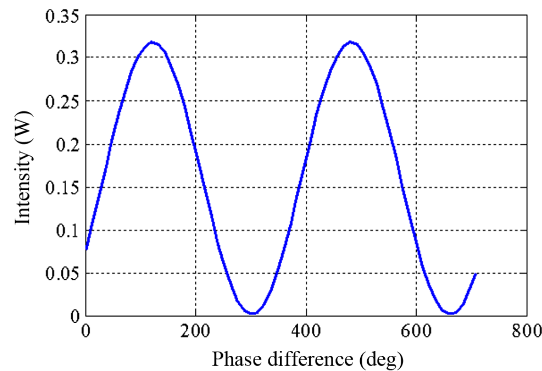

Fig. 5 Simulation result of the intensity and phase difference.

2.2.2 *Interface weight analysis of ghost reflection*

For heterodyne interferometer, ZEMAX simulation has no time concept and no heterodyne frequency. That is, the software cannot provide heterodyne interferometry directly based on phase demodulation, nor can it be used to simulate ghost reflection error. Although ZEMAX ray tracing software has no time series, its initial phase can be changed. Based on the interactive extension of ZEMAX and MATLAB, by self-determining a time series and giving the initial phase a change over time, the following phase changes can be obtained through reasonable parameter settings to simulate the heterodyne interferometer dynamic signal:

$$\theta_1 = 2\pi\Delta f t,$$
$$\theta_2 = 0, \tag{17}$$

where Δf is the frequency difference of the two beams, t is the time, and $2\pi\Delta f t$ is the phase difference of the two beams. Assuming that the initial phase of one of the beams is 0, the initial phase of the other beam is $2\pi\Delta f t$.

By substituting Eq. (17) into Eq. (1), it can be concluded that by giving the initial phase a constant time variable, ZEMAX ray tracing software can be used to provide simulation method in heterodyne interferometry. Figure 5 shows the relationship between signal strength and phase of the simulation model under ideal conditions.

The displacement measurement accuracy can be obtained by the difference between the actual set motion displacement of the reflector and the measurement results collected by the interferometer. First, the reflector in ZEMAX ray tracing software is driven by MATLAB to move at a known speed. After each displacement of the reflector, the intensity of the light of the detector is acquired and the data are stored. Then, the phase of the interference signal is inversed by the intensity of the light acquired by the detector. And the interference phase is converted into the measurement displacement to obtain the calculated displacement. After subtracting the calculated displacement from the known movement displacement, the measurement error Δz can be obtained. Figure 6 shows the measurement error curve when the ghost reflection of each interface is not considered in this structure, and the measurement error is about 0.12 nm. This error comes from the model establishment of other error sources except ghost reflection, such as tooling error and environmental error.

To provide the simulate of the angular tolerance with the interferometer structure, it is represented by AC/DC. First, the reflector in ZEMAX ray tracing software is driven by MATLAB to rotate along three axes at a certain angle, and the intensity of the light of the detector is collected after each rotation, and the data are stored. Then, the AC/DC is calculated using Eq. (8) offline through the collected intensity of the light of the detector data. By judging the range of AC/DC value, the angular tolerance can be obtained. As shown in Fig. 7, in the range of ± 1.5 mrad, when the ghost reflectivity of each interface is not considered, the variation line of AC/DC with the three direction axes is obtained. It can be seen that in the above rotation angle range, the minimum value of AC/DC is higher than 50%, and the average value is higher than 80%. Therefore, in this structure and working condition, the rotation angle tolerance is ± 1.5 mrad at least.

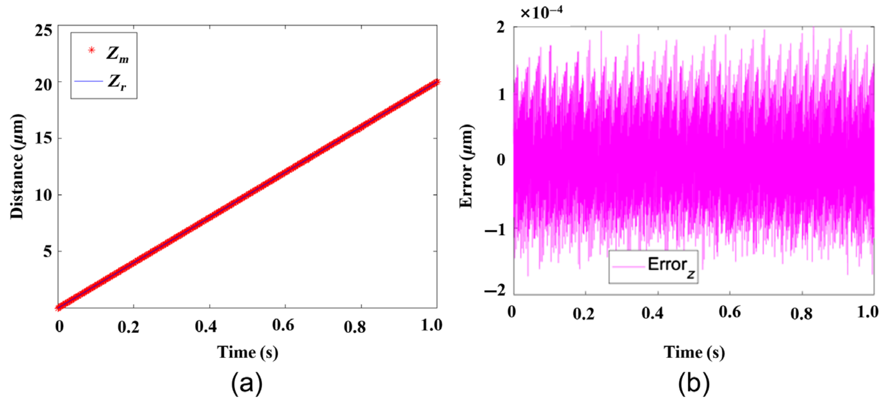

Fig. 6 Simulation result of the measurement error with displacement. (a) The displacement measured by the interferometer and the actual set motion displacement within 1 s. (b) The difference between the actual set motion displacement of the reflector and the measurement results collected by the interferometer.

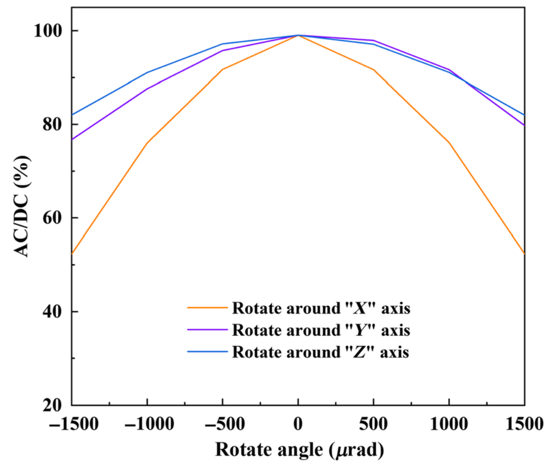

Fig. 7 Simulation result of the signal contrast with angular deflection varying in three directions of rotation.

As shown in Fig. 8, the AC/DC and measurement error changes of the known model under different ghost reflectivity are set by App Designer from 0% to 5%. It can be seen from Fig. 8(a) that with the increase of the ghost reflectivity from 0% to 2%, the average value of AC/DC received by the detector decreases, but it is not obvious. When the ghost reflectivity exceeds

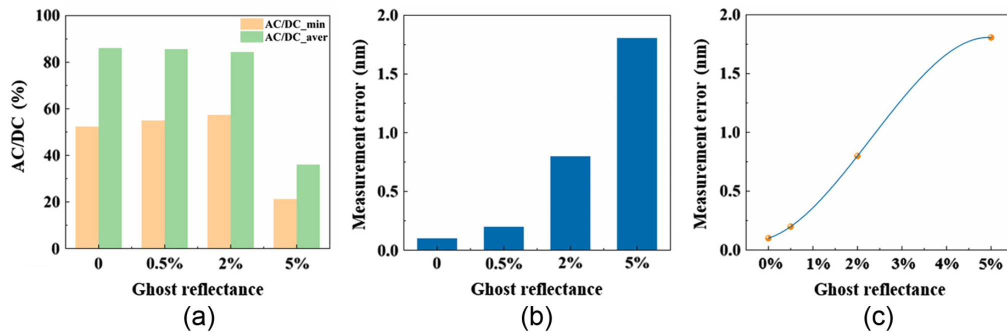

Fig. 8 (a) The relationship between simulation result AC/DC and ghost reflectivity ranges varying from 0% to 5% with all the interfaces. (b) Simulation result of the measurement error with reflectivity ranges varying from 0% to 5% with all the interfaces. (c) The variation curve of measuring accuracy with reflectance is fitted by third-order polynomial.

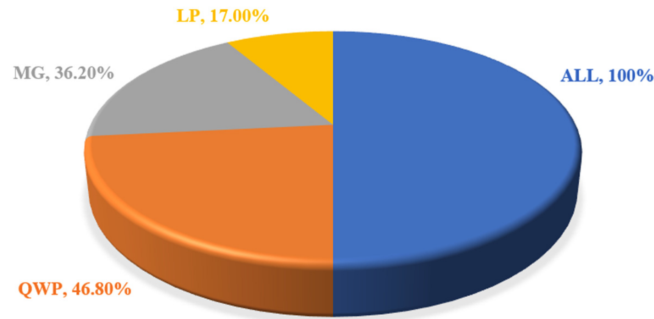

Fig. 9 Influence of different interface on measurement error weight proportion.

2%, the AC/DC of the interferometer under this structure decreases sharply, indicating that the structure can meet better interference signal quality within the range of ghost reflectivity below 2%. It can be seen from Fig. 8(b) that with the increase of the ghost reflectivity from 0% to 2%, the measurement error calculated by the intensity of the light of the acquisition detector increases significantly and almost exponentially. When it exceeds 2%, the growth rate of the interferometer measurement error under this structure slows down, but the error value is high, indicating that the measurement error is more sensitive to reflectivity than AC/DC. The curve fitting of measurement error with the change of reflectivity is performed, as shown in Fig. 8(c), and the functional relationship shown in the following equation is obtained. Through this equation, the measurement error of this structure interferometer under different reflectivity interfaces can be basically deduced

$$y = -23353x^3 + 1606.8x^2 + 12.17x + 0.0999. \tag{18}$$

It can be seen from Fig. 8(b) that when the ghost reflectivity is 0.5%, the measurement error of the interferometer is 0.2 nm. The influence weight of each boundary on the measurement error is tested by simulation with this reflectivity. By setting the ghost reflectivity of 0.5% on the App Designer interface, the weight analysis button of each interface is selected, and the backend program is called by the control variable method to modify the ghost reflectivity of each interface in ZEMAX. When only considering the first-order ghost, the influence of the reflectivity of different interfaces on the measurement error is obtained, as shown in Fig. 9. It can be seen from the diagram that the ghost reflection at QWP has the greatest influence on the measurement error of the structure, accounting for almost half of the measurement error. The second place is the mirror group [MG is made up of polarizing beam splitter (PBS) and CCR], and the influence accounts for 36%. The influence of linear polarizer (LP) is 17%, which is the smallest.

2.2.3 *Optimization algorithms and guides for the interferometer design*

Automatic ghost reflection interface searches and optimization design are proposed for the method. Based on the ZEMAX ray tracing software, the physical model of the optical path is established in this method, which can realize the function of optical tracking and the detection of interference intensity of the light. MATLAB software can be connected in ZEMAX ray tracing software so as to control the motion of the object to be measured in ZEMAX, acquire the intensity of the light of the detector, perform displacement calculation and error comparison, and change simulation parameters in ZEMAX, such as interface reflectance. In the part of optimization design, a genetic algorithm is applied to control the direction of optimization in MATLAB. The App Designer interface is a human–computer interaction used for automatic ghost reflection interface search and optimization design. By editing the visual interface, MATLAB functions are called and results are displayed. It greatly facilitates the operation of designers. The functional implementation module of this method is shown in Fig. 10.

The influence of ghost reflectivity on the measurement signal quality and measurement accuracy is simulated by controlling ZEMAX ray tracing software by MATLAB. It is known that the ghost reflection interface is the source of ghosts. To find the influence weight of ghost

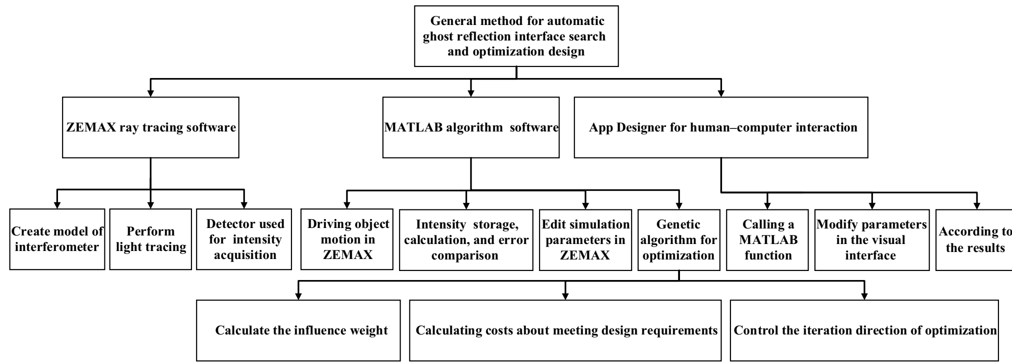

Fig. 10 Automatic ghost reflection interface search and optimization design function module diagram.

reflection on the interferometer more conveniently, an App Designer interface for human–computer interaction is established. App Designer is an environment for building MATLAB applications. As shown in Fig. 11, the interface is more comfortable than GUIDE after optimization and updating. By calling the MATLAB function and modifying parameters in the visual interface, it is more convenient to control ZEMAX ray tracing software and simulate the interferometer. First, setting all interfaces at the App Designer interface with the same ghost reflectivity, the ghost reflectivity is tested according to the actual reflectivity film of the optical element used in the actual manufacturing, such as 0.3% or 5%. Then, when the weight analysis function of different interfaces is selected in the program interface, the control variable method is used to perform the optical tracking simulation on each interface with two standards as the measurement

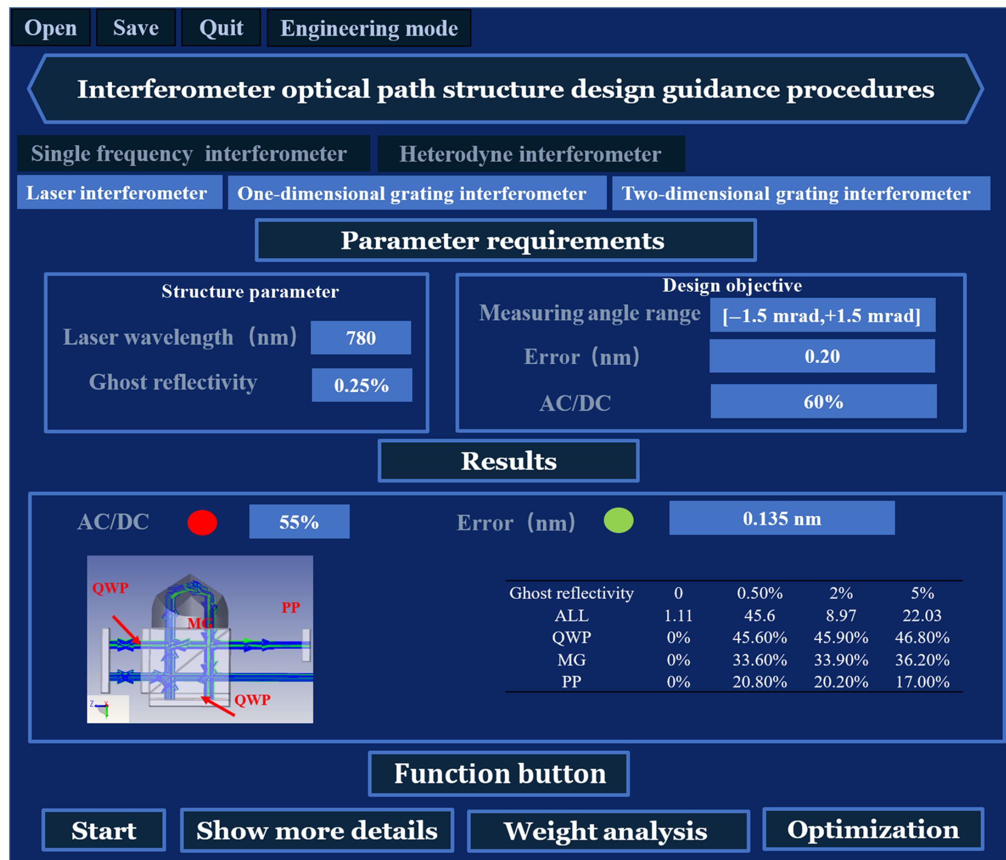

Ghost reflectivity	0	0.50%	2%	5%
ALL	1.11	45.6	8.97	22.03
QWP	0%	45.60%	45.90%	46.80%
MG	0%	33.60%	33.90%	36.20%
PP	0%	20.80%	20.20%	17.00%

Fig. 11 Diagram based on App Designer development for human–computer interaction program interface.

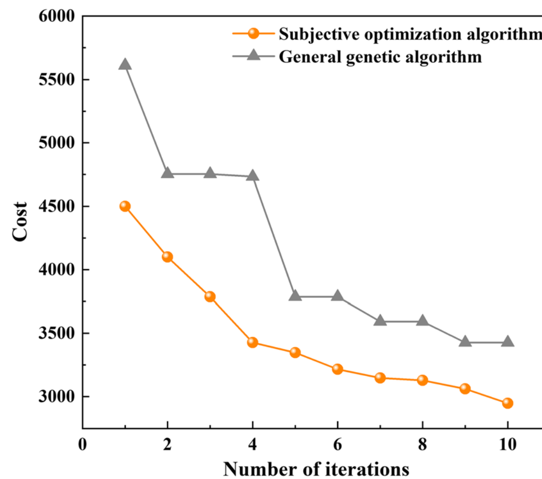

Fig. 12 Objective function curve of parameter optimization.

accuracy and AC/DC, so as to obtain the interface that affects the interferometer most seriously. Subsequently, it can be optimized by optimizing the component coating process or structural compensation. The program interface can also input the technical specification parameters of the interferometer according to the measurement requirements and output the range of ghost reflectivity of each interface that meets the given requirements after the optical tracking simulation in the program interface.

Without considering the manufacturing cost, when the reflectivity of all interfaces is the minimum, the measurement error of the interferometer obtained in the simulation is about 0.29 nm, in the range of ± 1.5 mrad, the minimum value of AC/DC is higher than 50%. With guaranteed technical specification that measurement error is about 0.31 nm and in the range of ± 1.5 mrad, the minimum value of AC/DC is higher than 50%. After optimization with the goal of reducing costs, several key interfaces for ghosting maintain high costs, and other interfaces reduce manufacturing costs obviously. Figure 12 shows that the optimization method maintains the measured technical specification within the acceptable range, but the manufacturing cost is reduced by about 45%, and after 10 iterations, on the premise of ensuring the technical specification, the overall optical element cost of the interferometer is significantly reduced, the optimization effect is improved by about 14% compared with the conventional genetic algorithm.

3 Quadruple Optical Subdivision Experiment

To verify the effectiveness of the above method, a traditional interferometer structure for ghost reflection identification and optimization, the structure is more integrated, quadruple optical subdivision is a suitable sample for method validation. The influence of stray light caused by ghost reflection in the interferometer on the measurement signal AC/DC and measurement accuracy was verified by experiments.

In the experiments, a typical quadruple optical subdivision interferometer was built as shown in Fig. 13. A linearly polarized 780 nm laser beam is incident on a PBS. Then the beam is divided into two parts: one beam passes through a QWP and points to a reference mirror, which was fixed and kept absolute static; and the other passing through another QWP enters the target mirror which was fixed on a precision stage. Both beams pass through QWP twice, and their polarization changes 90 deg, and they pass PBS in the opposite way before. Then two beams pass through the CCR and exit in parallel. Finally, the beams are incident on the reference mirror and the moving target mirror through PBS again. After returning, the beams interfere at the position of PBS. Finally, the interference beam enters the photodetector. The displacement in the experiment was realized by a precision piezoelectric platform (P-587, PI Inc.). The target to be measured was a plane mirror fixed on the upper precision piezoelectric motion platform.

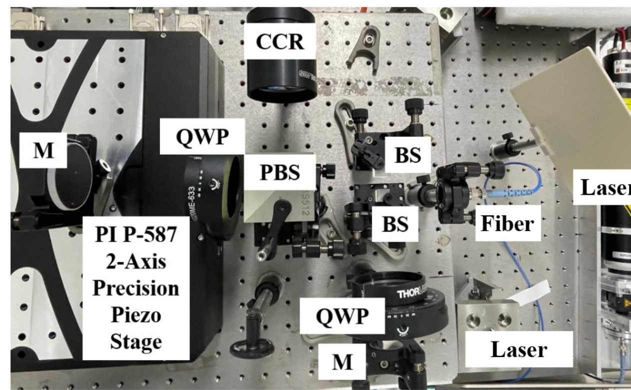

Fig. 13 Overall perspective of experiment setup.

To verify the influence of ghosts generated by the above ghost reflectivity on the AC/DC measurement signal and measurement accuracy of the interferometer, the interference signal obtained by the above interferometer is transmitted to the photoelectric detector for photoelectric conversion, and the digital oscilloscope is used to display the waveform of the interference signal. The interference signal waveform with the ideal condition is shown in Fig. 14(a). By converting the output signal into the measurement phase through the phase plate, the phase is resolved by the phase plate, and the obtained measurement phase is offline processed by MATLAB software to obtain the displacement. The measurement accuracy of the ideal situation is shown in Fig. 14(b). The measurement error in Z direction is 0.51 nm. The error comes from the motion error of the micro stage and the measurement error of the interferometer, which is in good agreement with the simulation results. Figure 14 shows the displacement measurement results of the grating interferometer with a sampling rate of 5 kHz. The experimental results were obtained within 1 s.

The errors affecting the interferometer include environmental errors, instrument errors, and so on. In this study, when changing the ghost reflection of the interferometer, it is assumed that other factors affecting the accuracy remain constant. To verify the influence of optical element interfaces with different reflectance on the measurement indexes of the interferometer, different types of PBS, QWP, CCR, and LP for different wavelength segments were used to build the interferometer with the same structure to verify the influence of ghost reflection. By testing different types of optical elements, the reflectance of QWP and MG is 0.3% and LP is 1% when the optical elements with the most ideal reflectance are used. The ghost reflectance of QWP and MG group is 1% and LP is 2%. Table 1 shows the experimental parameters of four different interface with nonideal reflectance experiments with the above optical elements.

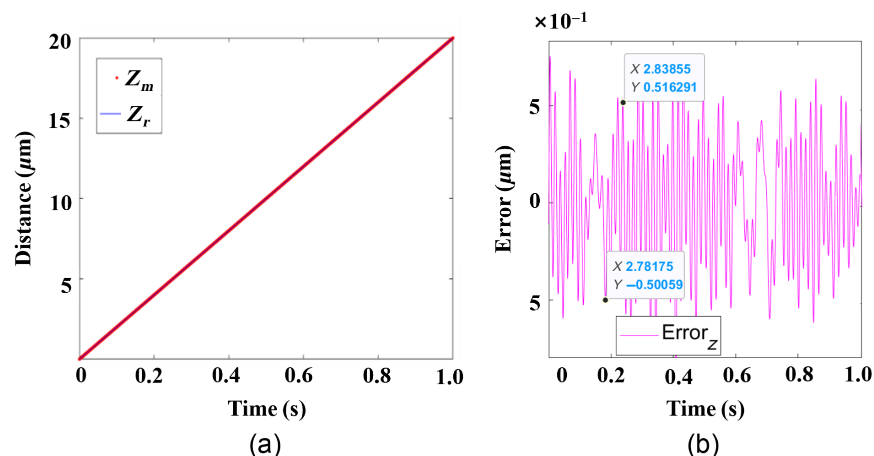

Fig. 14 (a) The interference signals obtained. (b) The measurement error obtained.

Table 1 Error with reflectivity in different experiment number.

Optical element	QWP	MG (PBS)	LP		
Experiment number	Reflectivity (%)			Total	Error (nm)
1	0.3	0.3	1	1.6	0.51
2	1	0.3	1	2.3	1.61
3	0.3	1	1	2.3	1.22
4	0.3	0.3	2	2.6	0.54

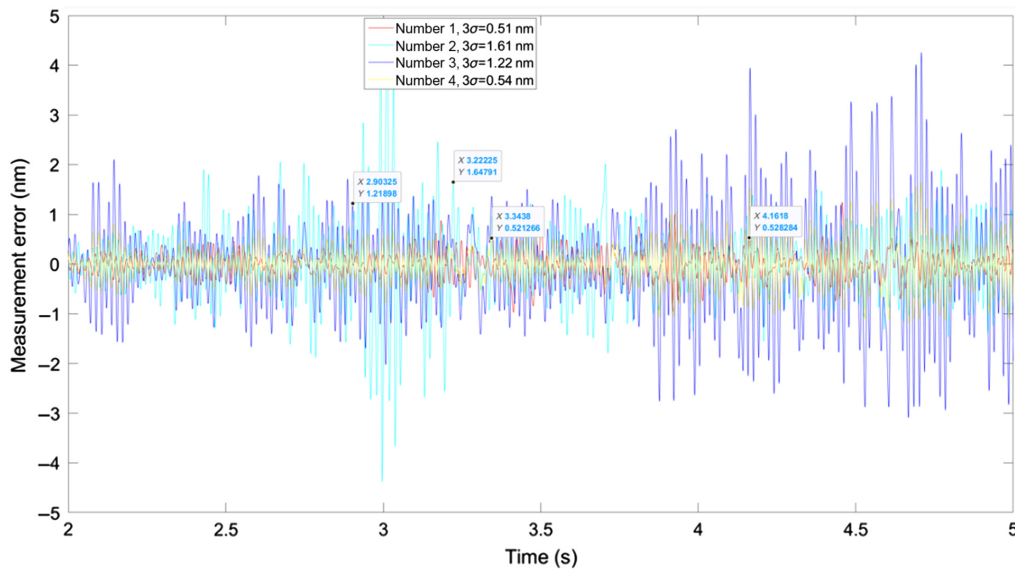

Fig. 15 Measurement errors of the different interface with nonideal reflectance.

Figure 15 shows the measurement errors in experiments with four different parameters in Table 1. It can be seen that the influence of QWP and MG with different transmittance (the MG in this structure only has PBS and CCR) and LP on the measurement accuracy of the interferometer is basically consistent with the trend of simulation results. By comparing experiments 1 and 2, it can be seen that the ghost reflection at QWP has the greatest influence on the measurement error of the structure. When the reflectance increases from 0.3% to 1%, measurement error increases by 216%. The second most influential is MG (in this structure, MG only has PBS and CCR). When its reflectance increases by the same amount, the measurement error increases by 139%. When the reflectance of LP increases from 1% to 2%, the measurement error increases by 6%. Therefore, the interferometer can take the interface reflectivity shown in experiment 4 to achieve a measurement error within 0.54 nm and the lowest manufacturing cost, thus providing guidance for the interferometer. With the premise of the lowest manufacturing cost, by analyzing the influence weight of ghost reflectivity on the interferometer measurement signal and measurement resolution, the nonideal position that mainly affects the interferometer measurement is identified and also verifies the rationality of the proposed optimization method.

4 Conclusions

We studied the influence of ghost reflection on the interferometer signal and measurement error used for the precision measurement of equipment such as a lithography machine workpiece table and proposed a general method for automatic ghost reflection interface identification based on

ZEMAX ray tracing software for research. To modify parameters in the visual interface, a program is applied based on App Designer to find the source of ghost reflection and analyze the influence weight. Finally, a typical interferometer model is used to verify the effectiveness of the proposed method. The results show that the ghost generated by the ghost reflection will affect the measurement signal and measurement accuracy of the interferometer. And the proposed method accurately reflects the influence weight of ghost reflection on interferometer interferometry. The interferometer can achieve a measurement error within 0.54 nm and maintain the lowest manufacturing cost. It can be proved that the ghost reflectance of the main optical elements in the interferometer will affect the measurement error, and QWP has the greatest impact on the structure of the interferometer.

Acknowledgments

We thank the Beijing Laboratory of Precision/Ultra Precision Manufacture Equipment and Control for its support in this work. This research was funded by Major National Science and Technology Project of China (Grant No. 2018ZX02101003). The authors declare no conflicts of interest.

Code, Data, and Materials Availability

Data underlying the results presented in this paper are not publicly available at this time but may be obtained from the authors upon reasonable request.

References

1. R. Heilmann et al., "Dimensional metrology for nanometre-scale science and engineering: towards sub-nanometre accurate encoders," *Nanotechnology* **15**, S504–S511 (2004).
2. F. Yang et al., "Two degree-of-freedom fiber-coupled heterodyne grating interferometer with milli-radian operating range of rotation," *Sensors* **19**, 3219–3230 (2019).
3. Z. Cheng et al., "Study on high accuracy displacement interferometer for lithography application," *Proc. SPIE* **5662**, 395–399 (2004).
4. Y. Xia et al., "Displacement calculation method for homodyne interferometers based on spatial phase delay of beams," *Opt. Eng.* **61**, 014106 (2022).
5. W. Ye et al., "Translational displacement computational algorithm of the grating interferometer without geometric error for the wafer stage in a photolithography scanner," *Opt. Express* **26**, 34734–34752 (2018).
6. C. Feng et al., "Accurate measurement of orthogonality of equal-period, two-dimensional gratings by an interferometric method," *Metrologia* **49**, 236–244 (2012).
7. J. Cui et al., "A method of calculating structural error in interferometer measurement system," *DEStech Trans. Comput. Sci. Eng.* **9471**, 201–205 (2016).
8. K. Creath, "Error sources in phase-measuring interferometry (invited paper)," *Proc. SPIE* **1720**, 428–435 (1992).
9. W. Ye et al., "Ultraprecision real-time displacements calculation algorithm for the grating interferometer system," *Sensors* **19**, 2409–2421 (2019).
10. A. El-Maksoud and H. Rania, "Ghost reflections of Gaussian beams in anamorphic optical systems with an application to michelson interferometer," *Appl. Opt.* **55**, 1302–1309 (2016).
11. R. Paschotta, *Encyclopedia of Laser Physics and Technology*, 2 Set., Wiley-VCH (2008).
12. H. Benard et al., "Simulation and analysis of ghost images for the megajoule laser," *Proc. SPIE* **3492**, 321–327 (1999).
13. J. Deng, X. Yan, and C. Zhou, "Eightfold optical encoder with high-density grating," *Appl. Opt.* **57**, 2366–2375 (2018).
14. C. Lin et al., "Two-dimensional diagonal-based heterodyne grating interferometer with enhanced signal-to-noise ratio and optical subdivision," *Opt. Eng.* **57**, 064102 (2018).
15. J. H. Shapiro and R. W. Boyd, "The physics of ghost imaging," *Quantum Inf. Process.* **11**, 949–993 (2012).

16. C. Zhao et al., "Ghost imaging LiDAR via sparsity constraints," *Appl. Phys. Lett.* **101**, 139–151 (2012).
17. B. Sun et al., "Normalized ghost imaging," *Opt. Express* **20**, 16892–16901 (2012).
18. P. Hu et al., "Nonlinearity error in homodyne interferometer caused by multi-order Doppler frequency shift ghost reflections," *Opt. Express* **25**, 3605–3612 (2017).
19. D. Köchert, J. Flügge, and C. Weichert, "Phase measurement of various commercial heterodyne He–Ne-laser interferometers with stability in the picometer regime," *Meas. Sci. Technol.* **23**, 4005–4012 (2012).
20. M. García, C. A. Acosta, and M. J. Mesa, "Genetic algorithms for mathematical optimization," *J. Phys. Conf. Ser.* **1448**, 012020 (2020).

Enming Zhang received his BS degree in mechanical engineering from Northwestern Polytechnical University of Materials Science and Engineering in 2020. He is a postgraduate candidate working on laser interferometers at Tsinghua University.

Weinan Ye received his PhD in mechanical engineering from Tsinghua University in 2020. He is an assistant researcher at Tsinghua University. His current interests include ultraprecision measurement and theory for ultraprecision systems.

Yizhou Xia received his BS degree in mechanical engineering from Huazhong University of Science and Technology in 2018. He is a PhD candidate working on laser interferometers at Tsinghua University.

Leijie Wang received his PhD in mechanical engineering from Tsinghua University in 2016. He is an assistant researcher at Tsinghua University. His current interests include ultraprecision measurement and theory for ultraprecision system.

Ming Zhang received his PhD in mechanical manufacturing and automation from Tsinghua University in 2005. He is a professor in the Department of Mechanical Engineering at Tsinghua University. His research interest is the design of ultraprecision motion stage of high-end semiconductor manufacturing equipment, including ultraprecision mechanical design and manufacturing, system modeling and analysis, and the design of high-precision linear motors and planar motors.